

Motivation

The central Tibetan Plateau was deformed, and possibly uplifted to near-modern elevations, prior to the Indo-Asian collision, analogous to the modern Altiplano-Puna Plateau in South America¹⁻¹³ (Fig. 1). Today, the Tibetan Plateau is roughly double the width of the pre-collisional deformation belt and the majority of post-collisional plateau expansion took place in the north.

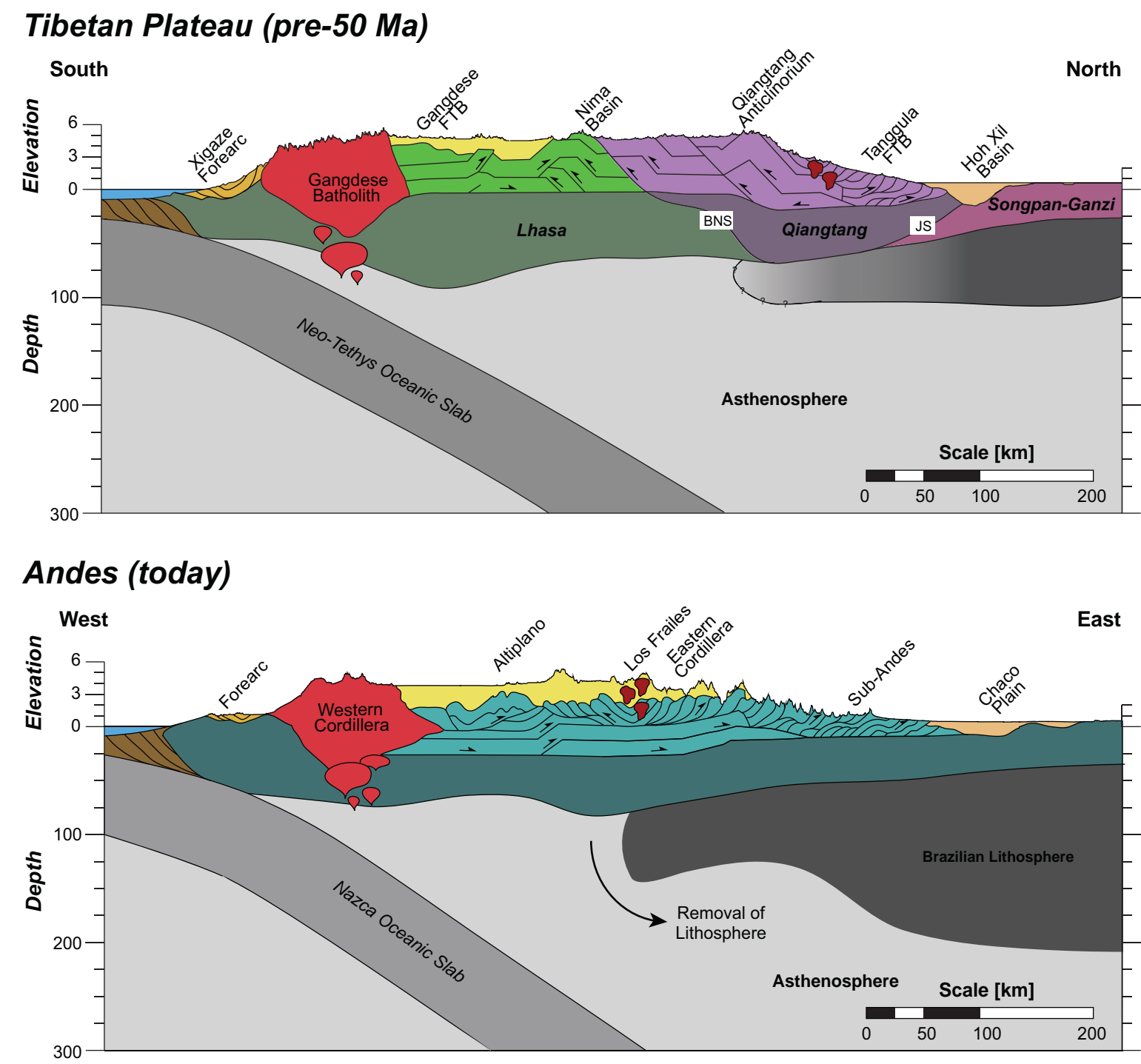
Outstanding Questions:

How and when was crustal shortening accommodated in northern Tibet?

How does the timing and magnitude of shortening compare with paleoelevation and modern values of crustal thickness?

What causal mechanisms for plateau uplift are consistent with our data?

Figure 1. Comparison of schematic cross sections of the pre-collisional Tibetan Plateau (top) and the modern Andes. The cross section for the Tibetan Plateau was constructed based on cross sections of the Gangdese Fold and Thrust Belt¹⁴, the Nima Basin¹⁵, the Qiangtang Anticlinorium¹⁶, the Tanggula Shan¹⁴, and Hoh Xil Basin¹⁵. The yellow shaded region above the deformed Lhasa Terrane represents the relatively undeformed Linzizong volcanic cover. The mantle lithosphere shown beneath the Songpan-Ganzi and Qiangtang Terranes is based on modern geophysical data¹⁶ and is speculative. The Andean cross section is modified from (17) and is taken as an east-west transect across central Bolivia.



The Fenghuoshan Fold and Thrust Belt

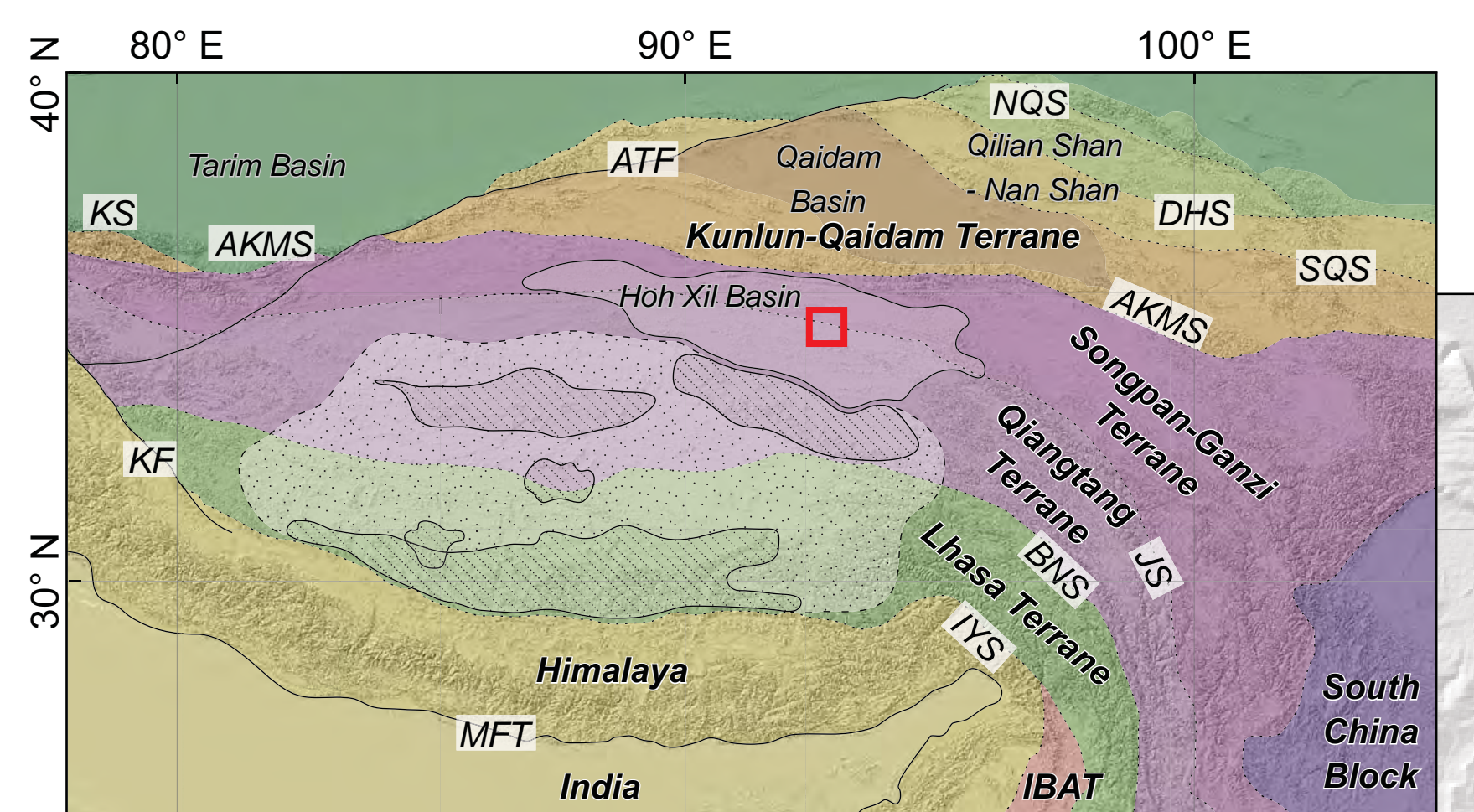
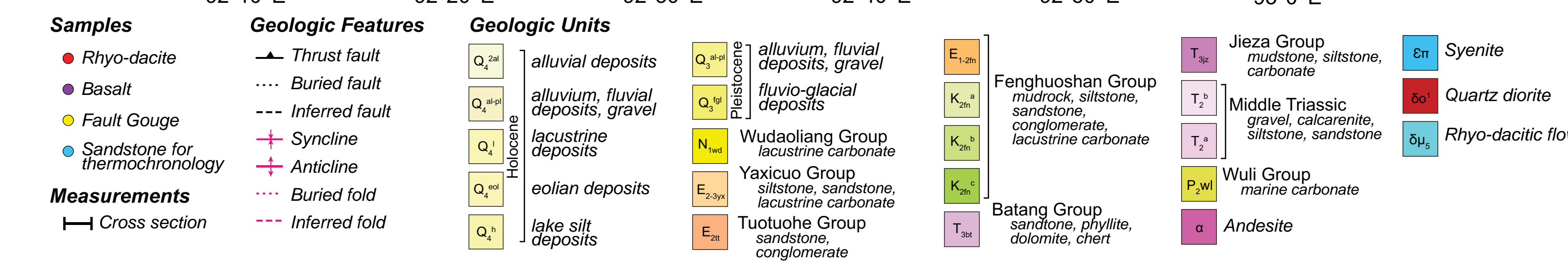
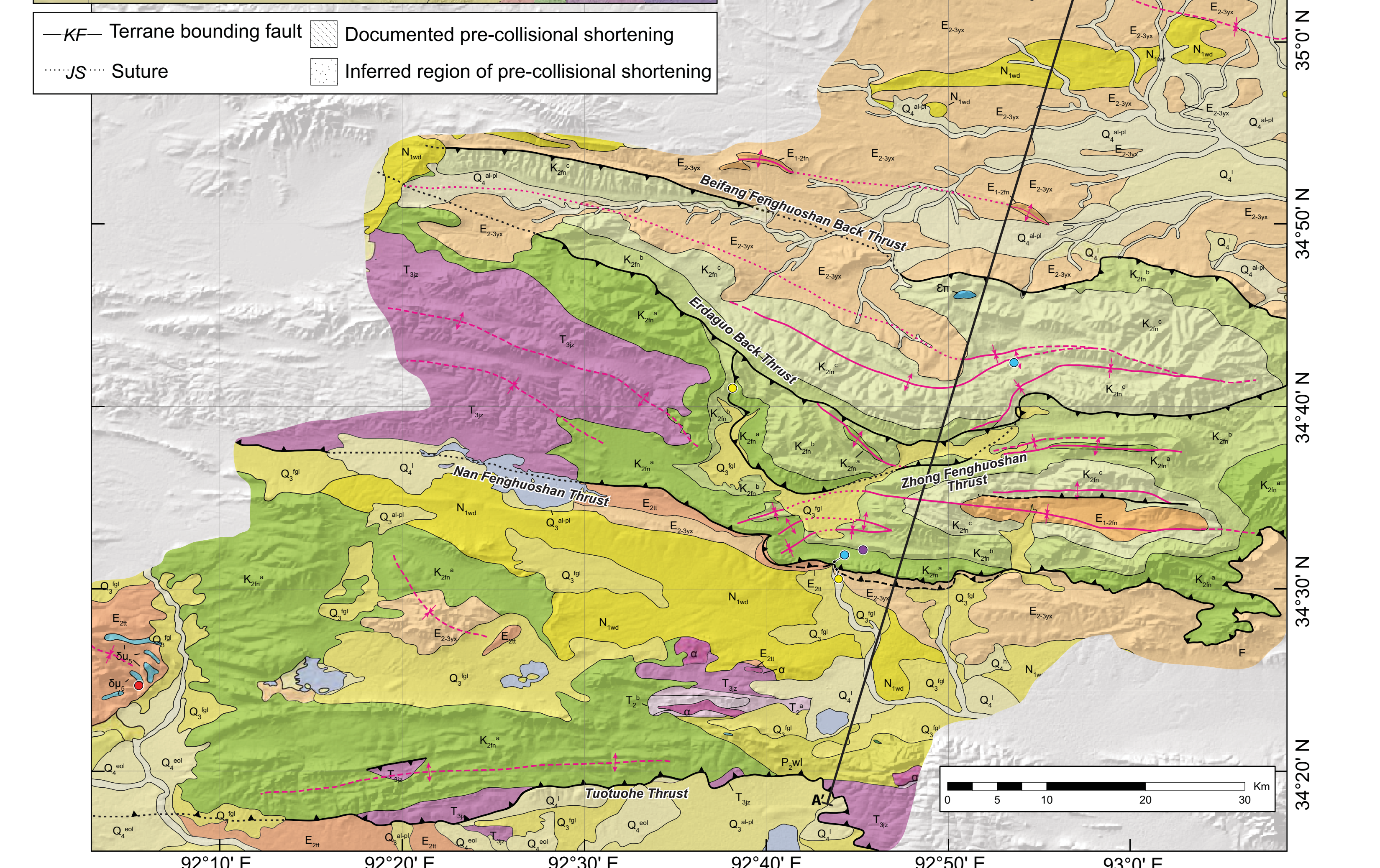


Figure 2. Inset: Terrane map of the Tibetan plateau. Regions of pre-collisional shortening are delineated in stippled and hatched overlay. The Hoh Xil Basin shown as white overlay. The Fenghuoshan Fold and Thrust Belt (FFTB) is located within the red box. Geologic map of FFTB based on original and published mapping¹⁸⁻¹⁹, of the central Hoh Xil Basin. Unit descriptions are along the bottom. Sample localities are overlain on the map. Structural cross section is indicated from A - A'.



Timing of Deformation

⁴⁰Ar/³⁹Ar GEOCHRONOLOGY

Sampling

We collected variably deformed volcanic rocks from the FFTB for geochronology (Fig. 2).

Results

The deformed rhyo-dacite is 33.46 ± 0.24 Ma (Fig. 3).

The lower flat-lying basalt is 27.33 ± 0.1 Ma (Fig. 3).

Interpretation

⁴⁰Ar/³⁹Ar ages indicate that north-south shortening of the FFTB ceased between ~34 and 27 Ma.

THERMOCHRONOLOGY

Modeling

We modeled apatite (U-Th)/He ages and apatite fission-track length distributions from samples collected from the FFTB (Fig. 2) using HeFTy²⁰. Constraints were compiled from the literature²¹.

Results

The onset of rapid cooling occurred by 45 - 48 Ma, followed by slow cooling in the Oligocene (Fig. 4).

Interpretation

Shortening and exhumation of the FFTB initiated in the mid-Eocene, soon after the onset of Indo-Asian collision, and continued into the Oligocene.

FAULT GOUGE DATING

Methods

We dated two thrust faults from the FFTB (Fig. 2). Fault gouge ages obtained by polype analysis and ⁴⁰Ar/³⁹Ar dating of clay-sized gouge aliquots and linear best fit using Bayesian regression techniques.

Results

Both fault gouge samples provide a faulting age of 44 - 45 Ma (Fig. 5).

Interpretation

We interpret this data to suggest that the south-directed thrust faults within the FFTB were active in mid-Eocene time.

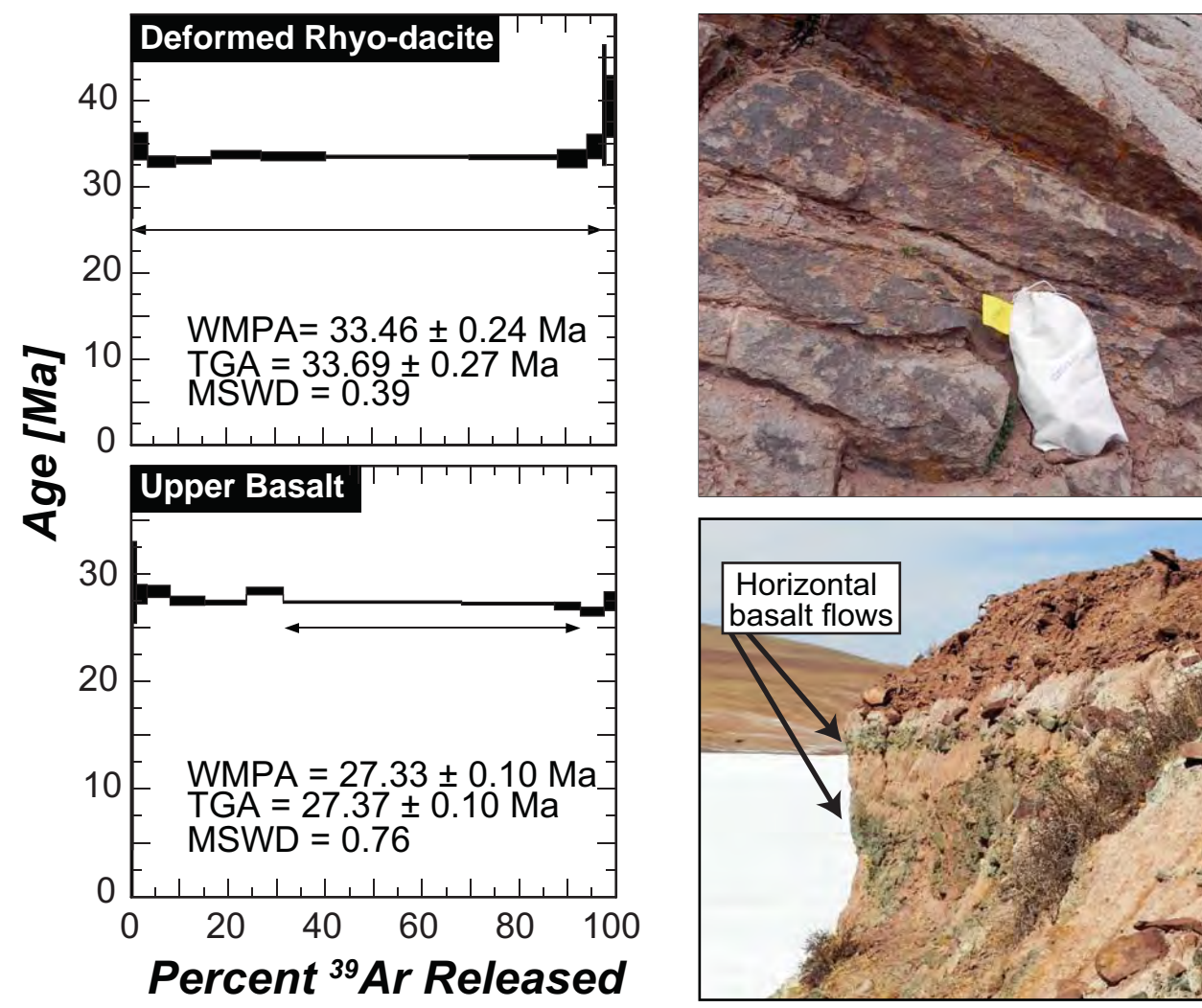


Figure 3. Outcrop photos and ⁴⁰Ar/³⁹Ar spectra for biotites separated from sampled volcanic units. Top photo and Ar spectra are for the deformed rhyo-dacite. Bottom Ar age spectra correlate to the lower horizontally oriented basalt flow. TGA: Total gas age. WMPA: weighted mean plateau age. MSWD: mean square weighted deviation.

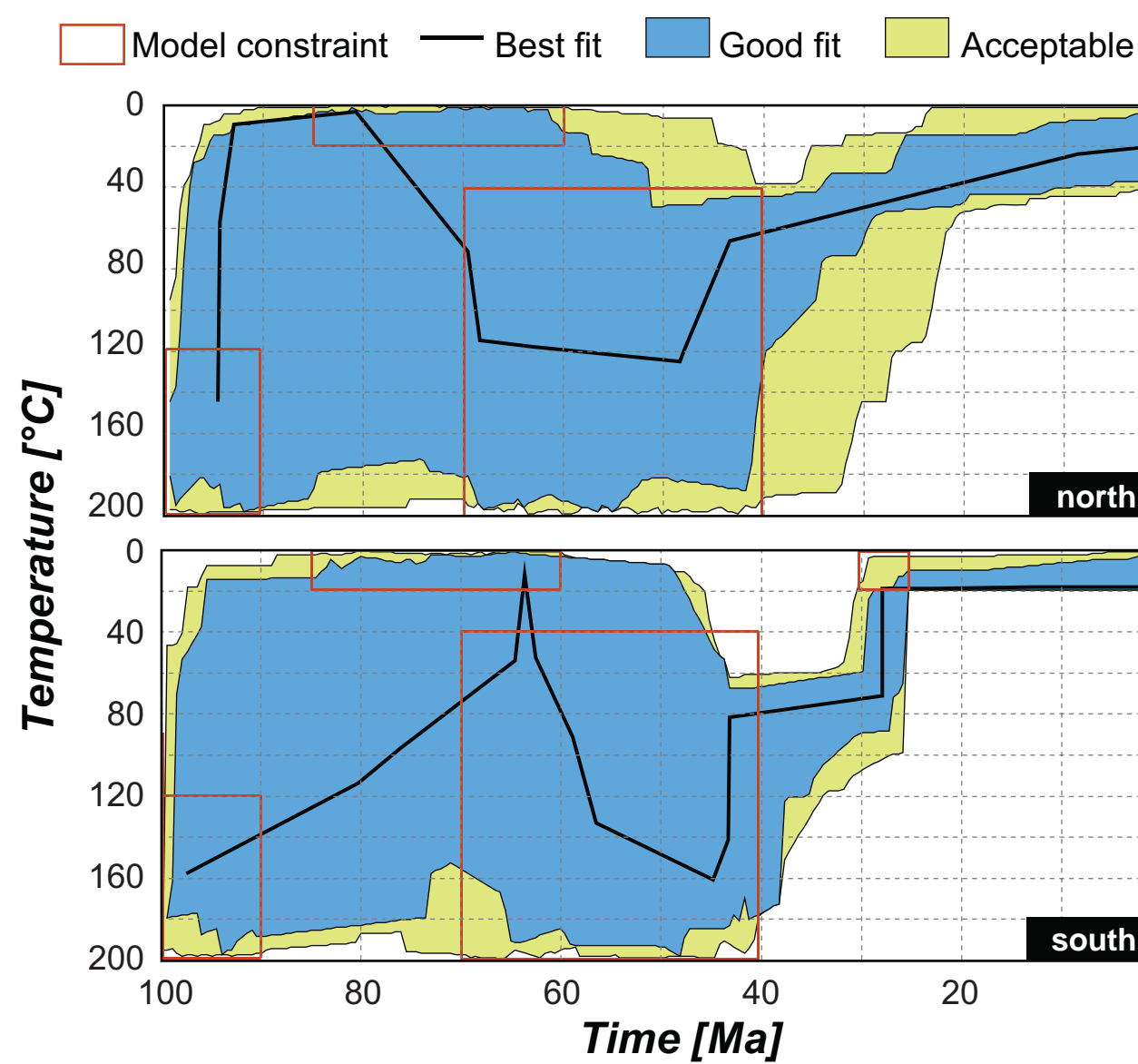


Figure 4. HeFTy model results for sandstone samples from the FFTB. Geologic constraints are based on deposition in the Cretaceous, subsequent burial in the Eocene, and (only for the southern sample) basalt eruption at the surface between 25-30 Ma.

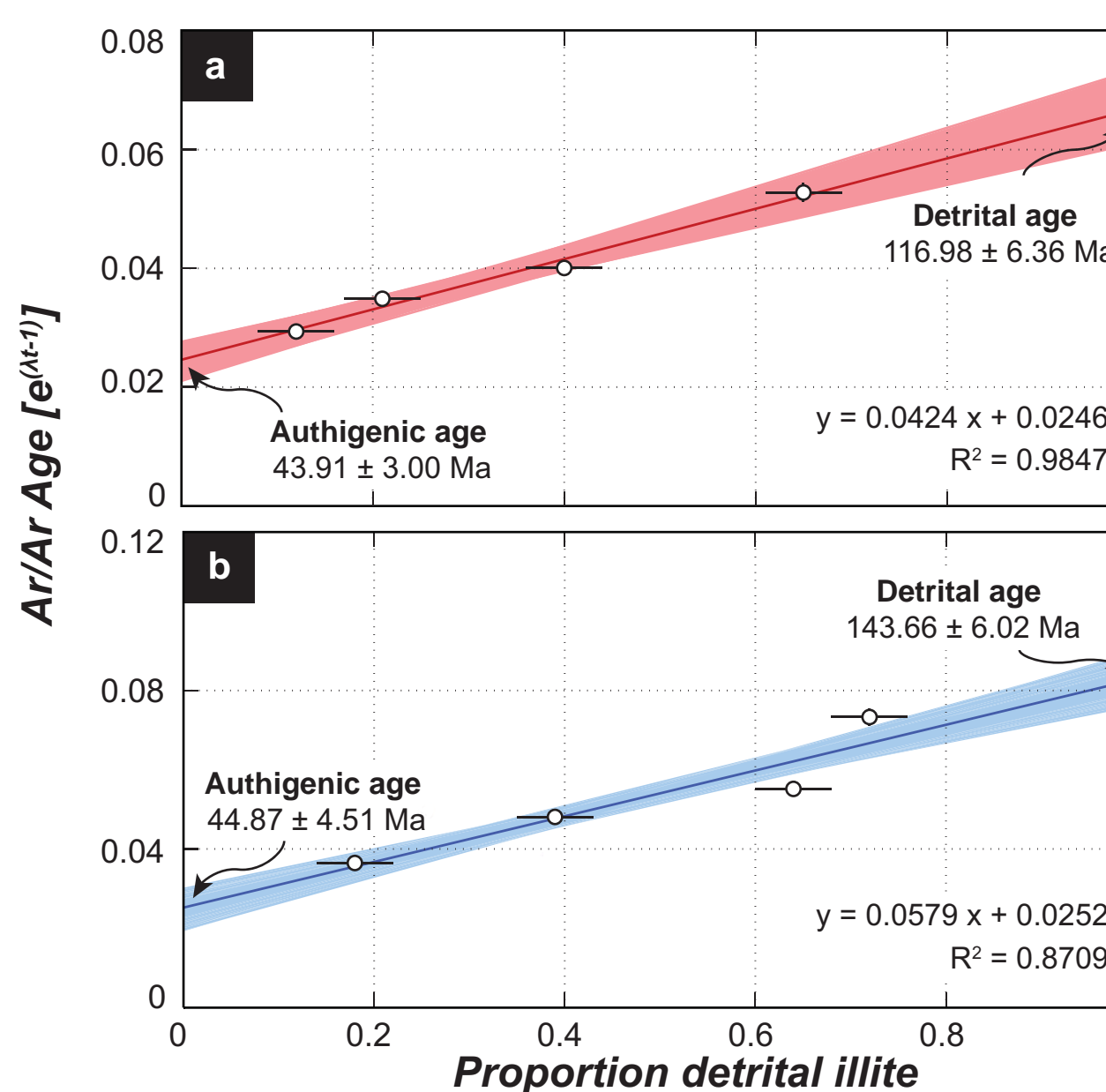


Figure 5. (A) Gouge aliquot ages plotted against illite concentrations for the Zhong Fenghuoshan Thrust fault (ZFT) and linear regression results. (B) Gouge aliquot age and illite concentrations for the Nan Fenghuoshan Thrust (NFT) and linear regression results.

Magnitude of Deformation

Methods

We constructed a geologic cross section across the FFTB (Figs. 2 and 6), based on field observations, isopach data¹⁵, and new and existing geologic mapping¹⁸⁻¹⁹. We line and area balanced the cross section to derive the amount of shortening and estimated uncertainties based on hanging wall cut-offs, depth to décollement, and stratigraphic thicknesses²²⁻²³.

Results

We derive a shortening estimate of 40.26 ± 10.03 km (28.0 ± 7.2%).

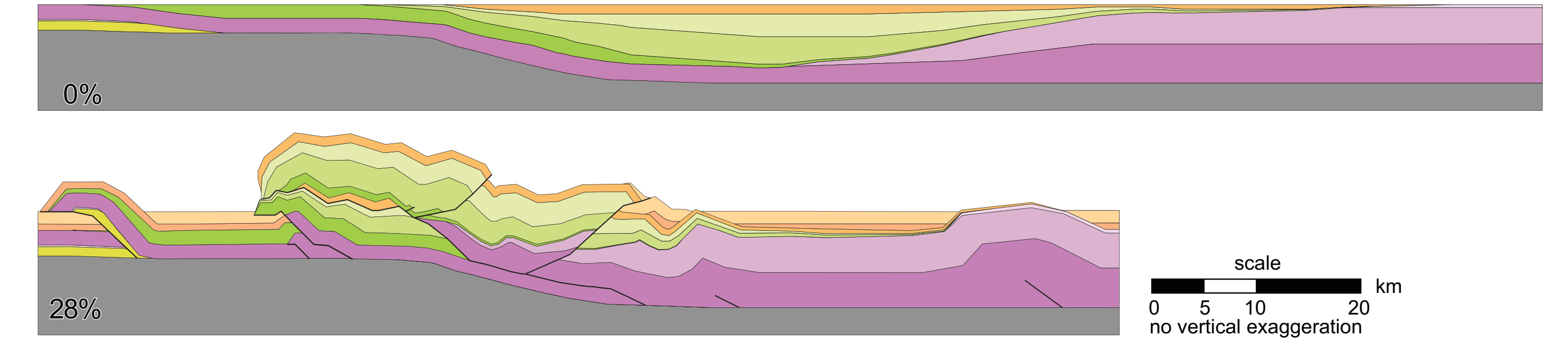


Figure 6. Cross section for the FFTB. Top panel shows undeformed cross section, reconstructed from isopach¹⁵ and stratigraphic data¹⁸⁻¹⁹. Bottom panel shows deformed range, constrained by structural measurements and field observations.

Isostatic Uplift

Methods

We calculate the isostatic uplift for ~28% pure shear to test whether shortening can account for modern crustal (65-70 km)²⁴ and lithospheric (130-150 km)²⁵ thicknesses and for Miocene paleoelevations (3.4-4.2 km)⁷.

Results

Measured upper crustal shortening cannot account for Miocene elevations or modern crustal thickness (Fig. 7b).

Interpretation

Other mechanisms of crustal thickening and surface uplift are necessary to build the northern plateau, such as lower crustal flow²⁶⁻²⁷, uniform lithospheric thickening²⁸⁻²⁹, and possibly mantle root loss³⁰ (Fig. 7c-f).

Isostatic calculations for proposed mechanisms for additional thickening and uplift are all compatible with reasonable initial crustal and lithospheric thicknesses (Fig. 7c-f).

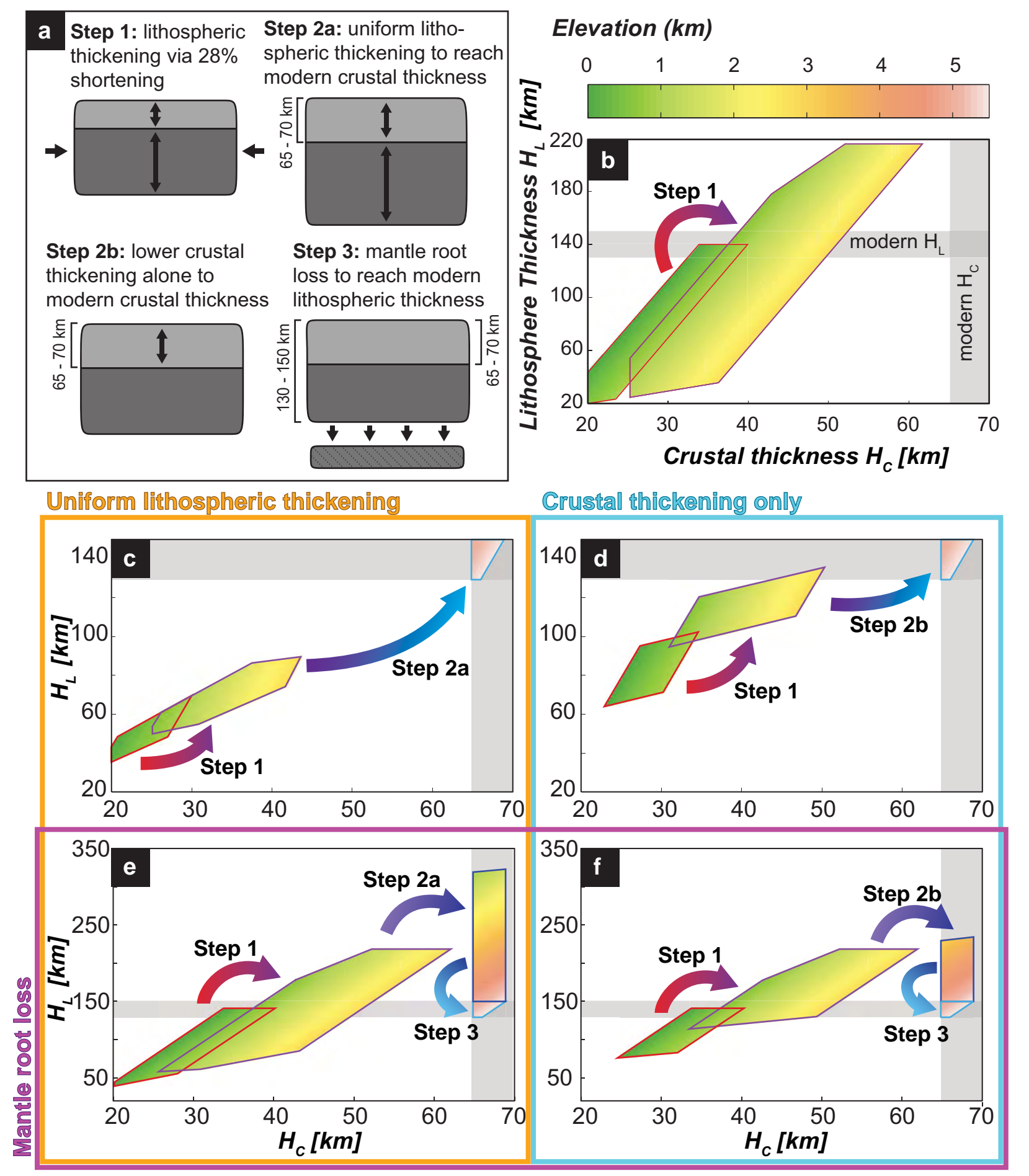


Figure 7. (a) Schematic diagrams of crustal thickening and/or uplift mechanisms explored in calculations of isostatic compensation. In plots (b-f), step numbers correlate to schematic figure (a) and results of surface uplift are colored by elevation. Initial crustal and lithospheric thicknesses are outlined in red, post-28% pure shear crustal and lithospheric thicknesses are outlined in purple, and final conditions following attainment of modern elevation and crustal and lithospheric thickness are outlined in cyan. Results for (b) uniform pure shear of 28.0 ± 7.2% assuming that the Hoh Xil Basin was originally below 1 km elevation, similar to modern retroarc foreland basins (c) uniform thickening to modern crustal and lithospheric thicknesses, (d) thickening of the crust only to modern crustal thicknesses, (e) uniform thickening and removal of the mantle lithosphere to modern lithospheric thickness (130 - 150 km)²⁵, and (f) over-thickening of the lithosphere via crustal thickening only and removal of the mantle lithosphere to modern lithospheric thickness.

Conclusions

Crustal shortening across northern Tibet

Crustal shortening initiated nearly synchronously across the northern plateau at the ~50 Ma onset of Indo-Asian collision.

Surface uplift

Uplift due to Eocene-Oligocene crustal shortening in the Hoh Xil Basin cannot reproduce high elevation and thick crust.

Paleoelevation⁷ and palynological³¹⁻³² data suggest high elevation was attained after the Oligocene, suggesting that additional uplift and crustal thickening occurred in the absence of upper crustal shortening.

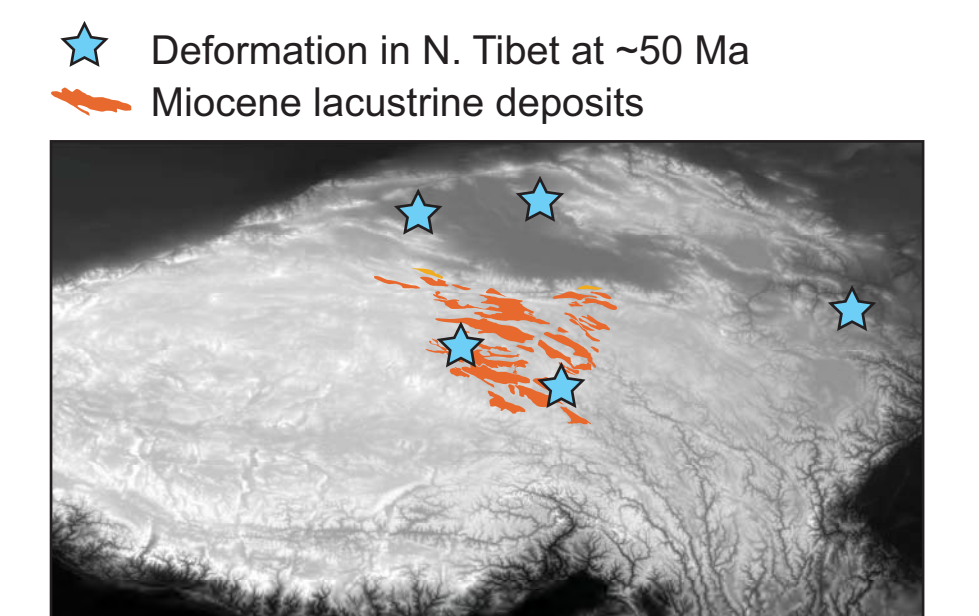


Figure 8. Crustal shortening at the onset of collision shown by blue stars, ~50 Ma deformation in northern Tibet is documented by (33, 34, 35, 36, 37). Miocene flat-lying lacustrine carbonate deposits are shown in orange³⁸.

Acknowledgments

This work was supported by NSF Continental Dynamics grants EAR-0908711 and EAR-1211434 to MKC and NAN and an NSF Graduate Research Fellowship awarded to LMS. We also acknowledge NSFC grant 40921120406 (to An Zhisheng) which supported both our Chinese colleagues at the Institute for Earth Environment and our joint fieldwork in Tibet.

References

- Burg et al., 1993, Eclogae Geologicae Helvetiae, 76(3), 643-665.
- England & Searle, 1986, Tectonics, 5(1), 1-14.
- Murphy et al., 1997, Geology, 25(8), 719-722.
- Kapp et al., 2005, GSA, 117(7), 865-878.
- Kapp et al., 2007a, GSA, 119(7-8), 917-933.
- Kapp et al., 2007b, GSA Today, 17(7), 4-9.
- Polissar et al., 2009, EPSL, 287, 64-76.
- DeCelles et al., 2007a, EPSL, 253(3-4), 389-401.
- DeCelles et al., 2007b, GSA, 119(5-6), 654-680.
- Rowley & Currie, 2006, Nature, 439, 677-681.
- Rohrmann et al., 2012, Geology, 40(2), 187-190.
- Xu et al., 2013, EPSL, 362, 31-42.
- Ding et al., 2014, 392, 250-264.
- Li et al., 2012, Gondwana Res., 22, 482-492.
- Liu et al., 2001, 71(6), 971-984.
- Owens & Zandt, 1992, Nature, 357, 37-43.
- McQuarrie et al., 2005, Tectonophysics, 399(1), 15-37.
- QBGMR (Qinghai Bureau of Geology and Mineral Resources), 1998a, Geologic map of the Cuoredejeia region, scale 1:200,000.
- QBGMR, 1998b, Geologic map of the Tuotuohe region, scale 1:200,000.
- Ketchum, 2005, Reviews in Mineralogy and Geochemistry, 59(1), 275-314.
- Staisch et al., 2014, Tectonics, 33(3), 281-301.
- Dahlstrom, 1969, Can. J. Earth Sci., 6, 743-757.
- Judge & Almendinger, 2011, J. Struct. Geol., 33, 458-467.
- Braltenberg et al., 2000, J. Geodynam. Evol., 489-505.
- Zhao et al., 2011, Nature Geosci., 4(12), 870-873.
- Clark et al., 2005, Geophys. J. Int., 162(2), 575-590.
- Karplus et al., 2011, J. Geophys. Res., 116, B07301.
- Isacks, 1988, J. Geophys. Res., 93, 3211-3231.
- Gubbeis et al., 1996, Geology, 24, 695-698.
- Molnar, P., P. England, and J. Martinod, 1993, Rev. Geophys., 31(4), 357-398.
- Duan et al., 2007, Earth Sci. J. China, 32(5), 629-637.
- Duan et al., 2008, Acta Micropaleont. Sin., 25(2), 185-195.
- Clark et al., 2010, EPSL, 296(1-2), 78-88.
- Duvall et al., 2011, EPSL, 304(3-4), 520-526.
- Horton et al., 2002, GSA, 114(7), 771-786.
- Yin et al., 2002, GSA, 114(10), 1257-1295.
- Yin et al., 2008, GSA, 120(7-8), 813-846.
- Wang et al., 2008, PNAS, 105(13), 4987-4992.